npj | quantum materials

Article

Published in partnership with Nanjing University

https://doi.org/10.1038/s41535-024-00666-y

Spin and lattice dynamics of the two-dimensional van der Waals ferromagnet CrI_3

Jonghyeon Kim[1,8], Saikat Banerjee[2,3,8], Junghyun Kim[4,5,8], Minseong Lee[6,8], Suhan Son[4,5], Jangwon Kim[1], Taek Sun Jung[1], Kyung Ik Sim[7], Je-Geun Park[4,5] ✉ & Jae Hoon Kim[1] ✉

Chromium tri-iodide (CrI_3) is a prototypical ferromagnetic van der Waals insulator with its genuinely two-dimensional (2D) long-range magnetic order below 45 K demonstrated recently. The underlying magnetic anisotropy has not been completely understood while both the Dzyaloshinskii-Moriya (DM) interaction and the Kitaev−Γ type interaction have been considered as the relevant magnetic Hamiltonian. In addition, the relation between the crystal structure and the magnetic order needs to be further elucidated concerning their possible coupling in few-layer samples and in the topmost surface layers of bulk samples. Here, we investigate these issues via temperature- and magnetic field-dependent terahertz spectroscopy on bulk CrI_3 single crystals, focusing on the dynamics of ferromagnetic resonances (FMRs) and optical phonons in the terahertz (THz) region from 4 to 120 cm^{-1} (from 0.5 to 15 meV). We narrow down the possible ranges of the interaction parameters such as the off-diagonal symmetric terms and the single-ion anisotropy. The accurate values of these parameters significantly constrain the magnitude of possible Kitaev−Γ exchange interaction and the topological magnon gap. Moreover, the structure-magnetism relationship was critically analyzed based on the temperature- and field-dependences of two E_u in-plane optical phonon modes, which shows that the commonly believed structural phase diagram of CrI_3, derived from surface-preferential data, has to be seriously modified.

Two-dimensional (2D) magnetism has been recently demonstrated in antiferromagnetic $FePS_3$[1] and ferromagnetic CrI_3[2] and $Cr_2Ge_2Te_6$[3] monolayer sheets exfoliated from bulk crystals. These observations violate the celebrated Mermin-Wagner theorem[4], which precludes long-range magnetic order in one- or two-dimensional systems at finite temperatures within the isotropic Heisenberg model with short-range interactions. The ensuing theoretical effort to establish strong magnetic anisotropy as a critical ingredient to overcoming spin fluctuations at finite temperatures required a detailed understanding of the magnetic Hamiltonian $\mathcal{H}$. Naturally, the possible roles of both the Dzyaloshinskii-Moriya (DM) interaction[5,6] and the Kitaev−Γ type interaction[6,7] have been extensively investigated. The former was discussed in the context of the topological protection of a Dirac point in the magnon band in CrI_3[5,6]. At the same time, the latter received much attention in several schemes to realize a quantum spin liquid (QSL) state in 2D CrI_3[6,7]. Thus, the experimental determination of the DM or Kitaev−Γ type interaction parameters is crucial in our overall understanding of the 2D ferromagnetism in CrI_3.

In addition, there exist several challenging yet important issues related to the crystal structure of CrI_3 governed by temperature and external magnetic field. Bulk CrI_3 has a monoclinic structure ($C2/m$) above the structural phase transition temperature (T_S) of 210 K but switches to a rhombohedral structure ($R\bar{3}$) below T_S[8]. This structural phase transition characterized by X-ray diffraction shows an anomalously broad temperature interval with a possible indication of coexisting phases[8]. On the other hand, the Ising-type ferromagnetic order sets in abruptly below the Curie temperature (T_C) of 61 K in bulk CrI_3 (Supplementary Note 2).

[1]Department of Physics, Yonsei University, Seoul, 03722, Republic of Korea. [2]Theoretical Division, T-4, Los Alamos National Laboratory, Los Alamos, NM, 87545, USA. [3]Center for Materials Theory, Rutgers University, Piscataway, NJ, 08854, USA. [4]Center for Quantum Materials, Seoul National University, Seoul, 08826, Republic of Korea. [5]Department of Physics and Astronomy, Seoul National University, Seoul, 08826, Republic of Korea. [6]National High Magnetic Field Laboratory, Los Alamos National Laboratory, Los Alamos, NM, 87545, USA. [7]Center for Integrated Nanostructure Physics, Institute for Basic Science (IBS), Suwon, 16419, Republic of Korea. [8]These authors contributed equally: Jonghyeon Kim, Saikat Banerjee, Junghyun Kim, Minseong Lee. ✉e-mail: jgpark10@snu.ac.kr; super@yonsei.ac.kr

Surprisingly, few-layer CrI_3 encapsulated with hexagonal boron nitride (hBN) possesses a monoclinic structure even at low temperatures and exhibits layer-dependent antiferromagnetism (AFM) below 45 K[9–12]. Also, a recent report shows the structure-dependent magnetism of CrI_3 in the moiré pattern of twisted CrI_3[13]. Interestingly, a recent Raman study reports surface-limited AFM in otherwise ferromagnetic bulk single crystals of CrI_3[14]. With all these conflicting reports, at the moment, a complete structural phase diagram on the parameter space spanned by temperature and magnetic field has not been definitively established despite some preliminary proposals.

Here we present our terahertz time-domain spectroscopy (THz-TDS) study of the ferromagnetic resonance (FMR) and optical phonon dynamics that identifies the basic structure of the magnetic Hamiltonian of CrI_3 and resolves the issue of the anomalous structure-magnetism relationship to this material. Our FMR and phonon data have been acquired on bulk CrI_3 single crystals as a function of temperature (1.5–300 K) and magnetic field (up to 7 T). The FMR data allows us to precisely determine the magnon gap at the zone center ($\vec{k}=0$) and narrows down the range of values of the Kitaev interaction K, the symmetric off-diagonal exchange parameter Γ, the single ion anisotropy A_c, and the Dzyaloshinskii-Moriya interaction ($\vec{D}$). In contrast, the phonon data yields a complete picture of the structural and magnetic phase transitions in the temperature-magnetic field parameter space, locating the actual phase boundaries of bulk single crystal CrI_3. Our results establish terahertz spectroscopy as an effective tool to study 2D magnetism and structural transitions in van der Waals magnetic materials.

Results

Magnetic field dependence of ferromagnetic resonance (FMR)

The magnetic field component of pulsed terahertz light applies torque to the spins in CrI_3. The resulting ferromagnetic resonance can be studied by observing the terahertz absorption or emission, the latter signal being caused by the precession of the spins during their relaxation process. Because the spins in CrI_3 are initially aligned along the c axis with the Ising ordering (Fig. 1a), three experimental configurations with distinct relative orientations of the external magnetic field $\mathbf{B}_{ext}$, the magnetic field component $\mathbf{b}_{THz}$ of the incoming THz light, and the ferromagnetic ordering (the crystallographic c axis) are expected to show finite absorption or emission (Supplementary Note 2). Accordingly, we conducted our terahertz time-domain spectroscopy measurements in all these three configurations as a function of external magnetic field strength ranging from 0 to 7 T.

Figure 1b shows the ab-plane terahertz absorbance spectra of a 217 μm-thick CrI_3 single crystal at 1.5 K with the external magnetic field $\mathbf{B}^c_{ext}$ of 7 T along the c axis and the terahertz magnetic field $\mathbf{b}_{THz}$ along the a axis. The raw data (blue curve) contains three sharp peaks at 9 cm^{-1} (FMR), 85.5 cm^{-1} (P1 phonon), and 114.9 cm^{-1} (P2 phonon) on top of a broad background with interference fringes coming from multiple internal reflections within the sample (Supplementary Note 2). To eliminate the interference fringes in the absorbance spectrum, we applied fast Fourier transform (FFT) to isolate and cut out the frequency component associated with the interference fringes and then applied inverse fast Fourier transform (IFFT) to retain the three sharp peaks (Supplementary Note 2). The intrinsic

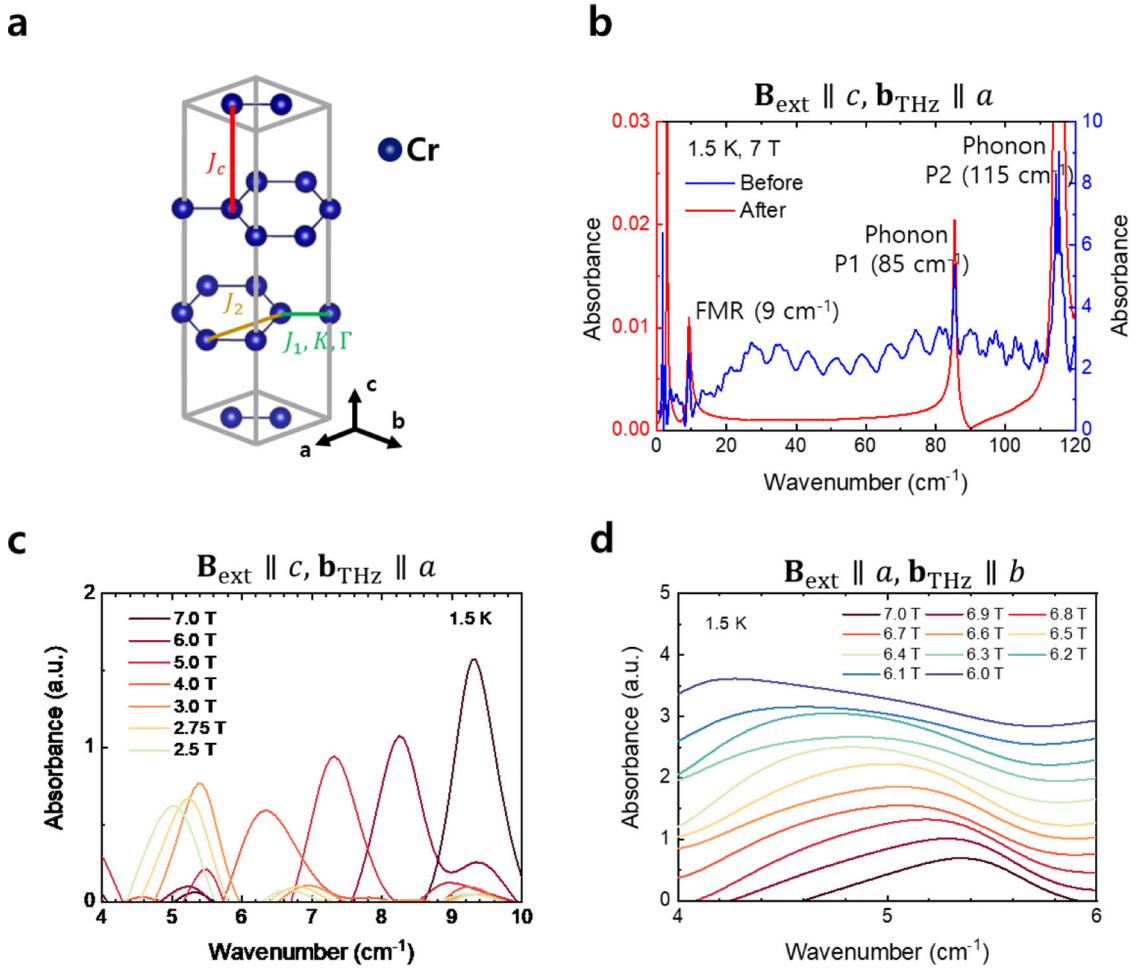

Fig. 1 | Crystal structure and magnetic field dependence of ferromagnetic resonance (FMR) in CrI_3 at 1.5 K. a Crystal structure of bulk CrI_3 in the low-temperature region (below $T_C = 61$ K). The blue spheres indicate Cr^{3+} cations; the iodide anions are not shown for clarity. **b** Absorbance spectra of a 217 μm-thick bulk CrI_3 crystal at 7 T and 1.5 K. Blue and red curves represent raw and post-processed data, respectively (see text). **c**, **d** Absorbance spectra near FMR at 1.5 K with an external magnetic field aligned along the c axis **c** and a axis **d** (the curves in (**d**) are shifted vertically for clarity).

absorbance spectrum (red curves in Fig. 1b) restored in this way exhibits somewhat distorted line shapes. However, their center frequencies are robust and can be analyzed further, including tracking of their field and temperature dependences. In particular, we identify the peak 9 cm^{-1} as a FMR absorption and the two peaks at 85.5 cm^{-1} (P1) and 114.9 cm^{-1} (P2) as infrared-active optical phonon modes of E_u symmetry. The vibrational patterns of the two phonon modes are shown in the inset of Fig. 3a, d[15]. In general, a FMR commonly occurs at frequencies in the low-frequency end of the terahertz region[16,17], much lower than to optical phonon frequencies. On the other hand, due to strong magnetic anisotropy and large anisotropic exchange energy[5,7], which generate a well-defined magnetic excitation gap, the FMRs in CrI_3 (both acoustic and optical branches) occur at higher frequencies (>135 cm^{-1}) compared to the FMRs of typical ferromagnets, such as EuO[18] and yttrium iron garnet[19], that fall into the microwave or submillimeter region.

Here, we focus on the lower-frequency (acoustic but gapped) FMR at 2.5 cm^{-1} at zero magnetic field. Having at hand an effective way to study the FMR and phonon modes, we now move on to determine the magnetic field (H) dependence of the FMR frequency at 1.5 K. Figure 1c shows a systematic blue shift of the FMR frequency as a function of magnetic field for the case of $\mathbf{B}_{ext} \parallel c$, $\mathbf{b}_{THz} \parallel a$, and $\boldsymbol{k} \parallel c$ (Fig. 1b and Supplementary Note 2). In this case, the FMR frequency follows a linear function with a slope of 0.97 cm^{-1} per Tesla (T) and a frequency intercept of 2.50 cm^{-1}. This type of FMR behavior is expected for the case of $\mathbf{B}_{ext}$ parallel to the magnetization axis ($\omega_{res} = \mu_0\gamma(H_{ext} + H_K)$ where ω_{res} is the FMR frequency, μ_0 is the vacuum permeability, γ is the gyromagnetic ratio, H_K is the effective anisotropy field, and H_{ext} is the external magnetic field)[20]. ω_{res} was located at 2.5 cm^{-1} ($\omega_{res} = (0.97 cm^{-1}/T) \cdot |\mathbf{B}_{ext}| + 2.50\ cm^{-1}$) at zero external magnetic field by using a linear extrapolation since our measurable frequency range was only above 4 cm^{-1}. The zero-field FMR frequency of 2.50 cm^{-1} compares well with 2.23 and 2.40 cm^{-1} as obtained for bulk and monolayer CrI_3 with electron paramagnetic resonance (EPR) and Raman spectroscopy[9,14,21,22], respectively. The case of $\mathbf{B}_{ext} \parallel a$, $\mathbf{b}_{THz} \parallel b$, and $\boldsymbol{k} \parallel c$ case is presented in Fig. 1d (Supplementary Note 2). Again, there is a systematic blue-shift of the FMR frequency with H, but our data are somewhat limited due to our low-frequency limit of 4 cm^{-1}. Consistent with our experimental data, the theoretical modeling predicts a nontrivial field dependence, as expected for the FMR in the case of $\mathbf{B}_{ext}$ perpendicular to the magnetization axis ($\omega_{res} = \mu_0\gamma\sqrt{H_K^2 - H_{ext}^2}$)[20]. Here we subtracted the absorbance at zero field from those measured under applied magnetic fields to enhance our FFT and IFFT data processing (Fig. 1c, d). In the direction of the magnetic field along the a axis $\mathbf{B}^a_{ext}$, we measured the FMR in a restricted magnetic field range above 6 T, again due to our low-frequency limit of 4 cm^{-1} (Fig. 1d). Finally, we note that the third experimental configuration of $\mathbf{B}_{ext} \parallel a$, $\mathbf{b}_{THz} \parallel a$, and $\boldsymbol{k} \parallel c$ does not allow for FMR excitation as the spins are easily forced to lie along the a axis by $\mathbf{B}^a_{ext}$ and do not couple with the incoming terahertz magnetic field of $\mathbf{b}_{THz} \parallel a$ (Supplementary Note 2).

Our FMR data can be utilized to help establish the key parameters of a candidate spin Hamiltonian proposed to describe the magnetic dynamics of CrI_3. The Hamiltonian first suggested in Ref. 5. consists of the superexchange interaction, the antisymmetric interaction (Dzyaloshinskii–Moriya (DM) interaction to explain the topological aspect of the magnon band), and the single-ion anisotropy. Therein, the combination of the DM interaction and the single-ion anisotropy explains the overall magnetic anisotropy despite some uncertainty regarding the size of the magnon gap[23]. In contrast, the so-called Heisenberg–Kitaev (J-K-Γ) Hamiltonian, proposed by Chen et al. in Ref. 6. and Lee et al. in Ref. 7, consists of the superexchange interaction, the bond-dependent Kitaev exchange interaction, and the symmetric off-diagonal exchange interaction (the Γ term). In this case, the Γ term determines the magnetic anisotropy responsible for the long-range ferromagnetic order and hence the magnetic excitation gap. A previous experimental study of the angle-dependent FMR has claimed that the FMR mode is well described by the J-K-Γ Hamiltonian[7], which also attempted to explain the magnetic excitations captured by inelastic neutron scattering[6]. Indeed, several microscopic theories point to the strong spin-orbit coupling induced by the heavy I atom as the main source of the bond-dependent anisotropic exchange interactions such as the Kitaev and Γ interactions[24]. Indeed, the DM interaction model may possibly explain FMR data, and the terahertz spectroscopy, relevant to the zero-wave vector excitations, may not fully validate either of the two magnetic Hamiltonians. Here, if the Γ term exists, the single-ion anisotropy should exist together because they both originate from the weak trigonal compression of the CrI_6 octahedra perpendicular to the plane. Also, in both models[6,7], DM interaction is symmetrically allowed between next nearest-neighbors. Therefore, we combine the two aforementioned models[6,7] and derive the analytical expression for the energy gap at $\vec{k} = 0$ we observed from our FMR measurement at zero magnetic field as follows.

A generic magnetic Hamiltonian derived microscopically for a magnetic honeycomb lattice contains the nearest-neighbor exchange interactions, (J-K-Γ), with the Zeeman energy term. In addition, we also consider the single-ion anisotropy that originates from the weak trigonal compression of CrI_6 octahedra perpendicular to the plane (i.e., along the c axis):

$$\mathcal{H}_1 = \sum_{\langle ij \rangle}\left(J\vec{S}_i \cdot \vec{S}_j + KS_i^{\nu}S_j^{\nu} + \Gamma\left(S_i^{\mu}S_j^{\lambda} + S_i^{\lambda}S_j^{\mu}\right)\right) + A_c\sum_i\left(\vec{S}_i \cdot \hat{c}\right)^2 + \overleftrightarrow{g}\,\mu_B\sum_i \vec{B} \cdot \vec{S}_i \quad (1)$$

where (λ, μ, ν) represents a permutation of (x, y, z), the local coordinates of the iodine octahedron. The Heisenberg exchange interaction (J) denotes generic Heisenberg exchange interactions that include all possible intra-plane and interplane interactions denoted as J_1, J_2, and J_c in Fig. 1a. K and Γ are the nearest-neighbor Kitaev and symmetric off-diagonal exchange interactions, respectively. We assume that $K_x = K_y = K_z = K$ and $\Gamma_x = \Gamma_y = \Gamma_z = \Gamma$. The single ion anisotropy is denoted as A_c. In the Zeeman term, $\overleftrightarrow{g}$ is the g-factor tensor in (a, b, c) coordinates, and $\vec{B}$ is the external static magnetic field. We assume that the magnitude of spin is $|\vec{S}| = 3/2$ throughout the paper. To this Hamiltonian $\mathcal{H}_1$, we further add the effects of DM and off-diagonal asymmetric exchange interaction in $\mathcal{H}_2$

$$\mathcal{H}_2 = \sum_{\langle\langle ij \rangle\rangle}\vec{D}_c \times \left(\vec{S}_i \times \vec{S}_j\right) + \Gamma'\sum_{\langle ij \rangle}\left(S_i^{\nu}S_j^{\mu} + S_i^{\mu}S_j^{\nu} + S_i^{\nu}S_j^{\lambda} + S_i^{\lambda}S_j^{\nu}\right) \quad (2)$$

so that the total Hamiltonian is $\mathcal{H}_{total} = \mathcal{H}_1 + \mathcal{H}_2$. Based on our model, we derived analytical expression for the energy gap observed at zero wave vector $(\vec{q} = 0)$ as

$$\epsilon_{\vec{q}=0} = S|3\Gamma + 6\Gamma' + 2A_c| \quad (3)$$

The details of derivation and various analytic expressions of the energy at high-symmetry points in reciprocal space can be found in Supplementary Note 1). From Ref. 6, we first learn that $\{\Gamma, A_c, \Gamma'\}$ determines the FMR frequency. We note that the DM term does not contribute to this magnon energy gap. Therefore, our calculation shows that $S|3\Gamma + 6\Gamma' + 2A_c| = 2.5\ cm^{-1}$ (0.31 meV) and g_c from the slope is about 2.1. The previous references presented an individual Hamiltonian based on either FMR or neutron scattering[5–7,25,26]. However, we present the most general model of Hamiltonian and consider the effects of both Kitaev and DM interaction. We first determined the possible range of $\{\Gamma, A_c, \Gamma'\}$ that can explain the magnon energy gap observed in our FMR experiment. Then, we made a comparison with the existing magnon spectrum to narrow down the values of the parameters[27]. The detailed procedure can be found in Supplementary Note 1. We tentatively propose that the values of the parameters in our study are: $J = -2.0199$ meV, $K = 0.2132$ meV, $\Gamma = -0.0599$ meV, $A_c = 0.0467$ meV, $D_c = -0.0962$ meV, and $\Gamma' = 0.0467$ meV. Our result shows the Kitaev term is relatively small compared to those reported in other references, and that the topological magnon gap at the K point is primarily opened by the DM interaction (Supplementary Note 1). Although our calculations were performed independently, they are in general consistent with those of an earlier theoretical reference[28].

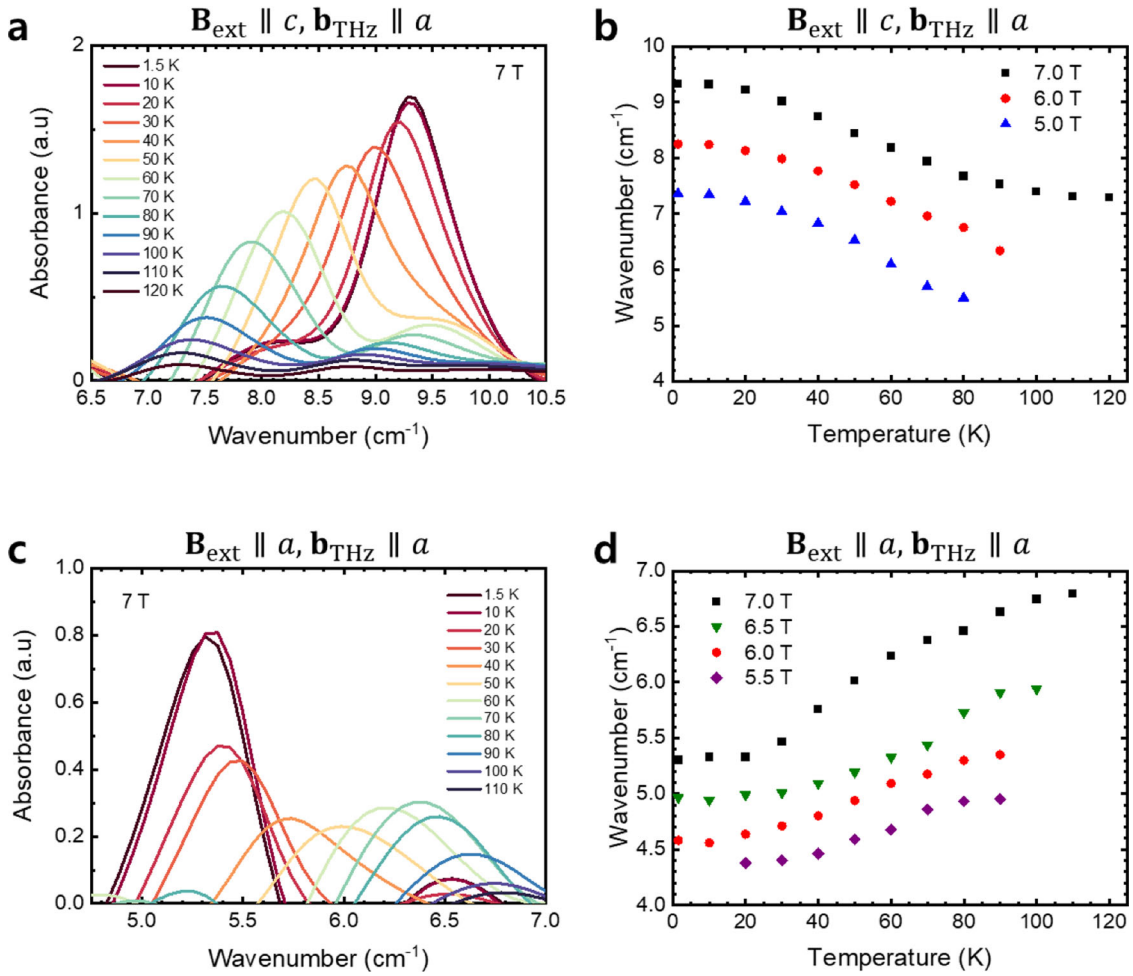

Fig. 2 | Temperature dependence of ferromagnetic resonance (FMR) of CrI_3. **a** Absorption spectra of FMR as functions of temperature at 7 T aligned along the *c* axis. **b** The peak position of FMR as a function of temperature under fixed external magnetic fields aligned along the *c* axis. Black, red, and blue symbols represent 7, 6, and 5 T, respectively. **c** Absorbance spectra of FMR as functions of temperature at 7 T aligned along the *a* axis. **d** The peak position of FMR as a function of temperature under fixed external magnetic fields aligned along the *a* axis. Black, olive, red, and violet represent 7, 6.5, 6, and 5.5 T, respectively.

Temperature dependence of FMR under a fixed external magnetic field

We also investigated the temperature dependence of FMR under a fixed external magnetic field. Figure 2a shows the absorbance spectra as a function of temperature under an external magnetic field of 7 T along the *c* axis (Fig. 2a) and the *a* axis (Fig. 2c). We subtracted the spectrum at 150 K (where no FMR was present) from the raw measured spectrum. The FMR systematically red-shifts for $\mathbf{B}_{ext} \parallel c$ as the temperature increases (Fig. 2a) because of the reduced magnetization by the enhanced thermal fluctuations[29]. The position of FMR was obtained via Lorentzian fitting (Fig. 2b) for $\mathbf{B}_{ext} \parallel c$. It was observed that FMR remained even above the Curie temperature T_C (61 K). We note that the temperature of 70 K corresponds to the inflection point for the temperature dependence of the FMR frequency (black squares in Fig. 2b). Under the external magnetic field $\mathbf{B}_{ext} \parallel c$ of 7 T, the spectral signature of FMR survives up to 120 K before it fades away. In connection with this observation, in the case of transition metal tri-halides, short-range ordering remains up to a temperature several times the Curie temperature under a strong magnetic field due to its low dimensional magnetism[8,30]. Therefore, the remnant magnetic resonance above T_C is assumed to be generated from enhanced short-range ordering in CrI_3 under a strong external magnetic field. In the case of $\mathbf{B}_{ext} \parallel a$, FMR was observed above T_C up to 110 K under the external magnetic fields of 7 T along the *a* axis (Fig. 2d). For magnetic fields in the range of 5.5–7 T, interestingly, the FMR frequency blueshifts with increasing temperature. As noted above, all the spins have been flipped to the *a* axis within the range of magnetic fields here. This peculiar blue shift with increasing temperature can only be explained by considering the coupling of the magnetic and lattice degrees of freedom. It could be speculated that a subtle interaction between the thermally activated lattice vibrations and the spins strongly polarized by the magnetic field increases the magnetic exchange coupling, which gives rise to an increase in anisotropic exchange energy.

Structural phase transition and phonons

CrI_3 has different crystal structures in bulk and in the two-dimensional limit at low temperatures[8,10,12]. Furthermore, the structure of few-layer CrI_3 at low temperatures may be affected by hBN encapsulation[9–12]. As the magnetic properties of CrI_3 itself depend sensitively on the stacking order, it is essential to verify the crystal structure of CrI_3 below T_C[31–33]. We investigated the temperature and magnetic field dependence of the two E_u phonon modes to confirm the structural evolution of the bulk state. First, the P1 phonon is very narrow and strong and is located at around 85.5 cm^{-1} at 1.5 K (Fig. 1b). We observed the temperature dependence of the position of the P1 phonon shown in Fig. 3a and confirmed the change due to the structural phase transition at T_S (~210 K)[8]. The P1 phonon moves to a lower-energy position as the temperature increases in the $R\bar{3}$ region, then jumps and splits to 80.3 cm^{-1} (P1-α) and 81.2 cm^{-1} (P1-β) at 209 K (Fig. 3a, b). The temperature of 209 K agrees with the structural phase transition temperature T_S (210 K)[8]. Furthermore, even with the application of a 7 T external magnetic field along the c axis, there was no alteration observed in the structural phase transition at 209 K (Supplementary Note 2). The

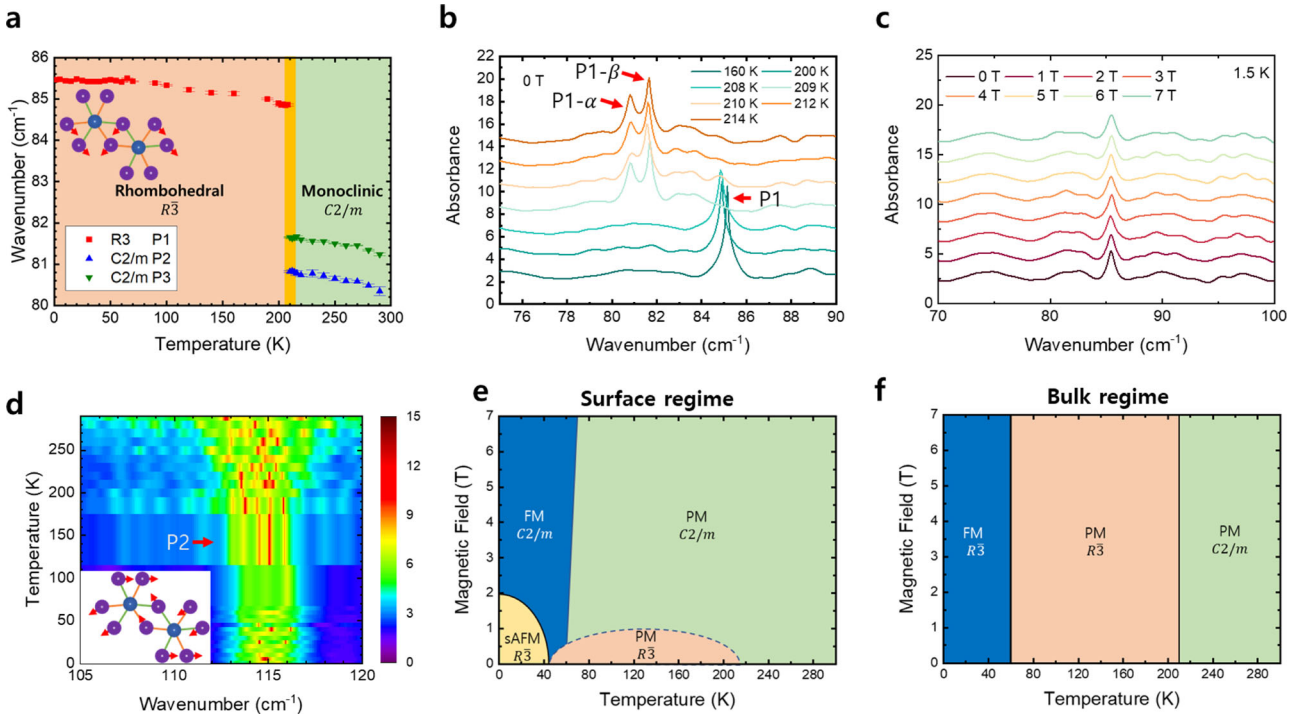

Fig. 3 | Phonon spectra and structural phase transition of CrI_3. a Position of phonon modes as a function of temperature from 1.5 to 290 K. Inset shows the vibrational direction of the P1 phonon mode. **b** Temperature dependence of phonon spectra (the curves are shifted vertically for clarity). **c** Absorption spectra of P1 phonon modes as a function of external magnetic field. (the curves are shifted vertically for clarity). **d** Color contour plot of phonon absorbance around 114.9 cm^{-1} with temperature from 1.5 to 290 K. Inset shows the vibrational direction of the P2 phonon mode. **e**, **f** Phase diagram of CrI_3 as a function of temperature and external magnetic field for bulk state according to the Raman measurement of Ref. 14. **e** and our terahertz results **f**. FM and PM denote ferromagnetic and paramagnetic, respectively. sAFM means surface antiferromagnetism.

temperature dependence of the P1 phonon was recently reported based on Fourier transform infrared spectroscopy (FTIR) experiment, but no significant structural phase transition was observed in contrast[34]. Table 1 shows our experimental results and the first-principles density-functional theory (DFT) calculation results for the two E_u phonon modes found at around 85.5 and 114.9 cm^{-1} [15,35]. The values of the E_u modes corresponding to the $R\bar{3}$ crystal structure of bulk CrI_3 agree with the calculations. Also, we found that these phonon modes are independent of the external magnetic field up to 7 T at 1.5 K, as shown in Fig. 3c.

The second E_u phonon mode, P2, located at 114.9 cm^{-1}, was also observed to change depending on the temperature and magnetic field shown in Fig. 3d. The very strong and broad absorption spectrum of the P2 phonon agrees well with the calculation of the high density of states[15] and the FTIR measurement[34] (Fig. 1b). We confirmed that the phonon mode shifted to lower energy with increasing temperature and gradually broadened above T_S (Fig. 3d). In the case of the P2 phonon, it was difficult to track any change with the external magnetic field because of the low transmittance and low signal intensity of the power spectrum (Supplementary Note 2). The longitudinal phonon mode ω_{LO} for P2 is expected to play an essential role in CrI_3, such as the origin of exciton-related polaronic character or for the magnon gap opening[36,37]. The P2 phonon observed in our experiment was the transverse mode (ω_{TO}). In general, a longitudinal mode can be estimated using the loss function $\mathrm{Im}(-1/\epsilon)$[38,39]. Therefore, we estimate that the longitudinal phonon mode ω_{LO} is located at 115.3 cm^{-1} at 1.5 K (Supplementary Note 2).

A previous Raman spectroscopy study reported the phase diagram of bulk CrI_3 depending on magnetic field and temperature[14] (Fig. 3e). In the case of the Raman experiment, the effect of approximately 30 outermost layers dominates even in a bulk sample, and approximately 20 outermost layers of CrI_3 have a surface layered antiferromagnetic state[40]. Based on this, it was assumed in ref. 14. that the $C2/m$ prevails at all temperatures under fields above about 1 T (Fig. 3e). However, our data indicate that $R\bar{3}$ persists between 50 and 210 K even for finite fields up to 7 T. Therefore, we assume that the Raman measurement probes the surface-dominated properties of CrI_3 (Fig. 3e). We suggest a modified phase diagram from the phonon behavior of bulk CrI_3 as shown in Fig. 3f. In the case of bulk CrI_3, the structural phase transition occurs at 209 K from the monoclinic to rhombohedral structure, and the crystal structure of CrI_3 is independent on an external magnetic field. Our results provide information on the structure and magnetism of bulk CrI_3, which will be helpful for future research.

Table 1 | Peak positions of E_u phonon modes dependending on the crystal structure

$R\bar{3}$ structure		$C2/m$ structure	
Bulk (cm^{-1})	**ML (cm^{-1})**	**Bulk (cm^{-1})**	**ML (cm^{-1})**
83	76, 81	77	82
85.5		**80.3, 81.2**	
107	105, 115	106	108
114.9	**115**	**114.2**	

In our experimental data, the phonon positions in the $R\bar{3}$ and $C2/m$ phases correspond to 1.5 K and 290 K, respectively. The bold values represent our experimental results. The other values are optical phonon frequencies from the first-principles density-functional theory (DFT) calculation[15,35]. ML means monolayer.

Discussion

In this study, we investigated the interaction of terahertz light with the spin and the crystal structure of a bulk CrI_3 single crystal by varying the temperature and external magnetic field. We demonstrated here that the precise temperature and external magnetic field dependences of the FMR data allow us to extract the range of Γ, Γ', and A_c, from the analytical expression derived from the most generic spin Hamiltonian for CrI_3. Our work is very much valuable because the determination of energy gap at $\vec{k} = 0$ with a high

resolution of our FMR measurement helps proposed parameters be accurately determined. For example, parameter sets determined by the inelastic neutron scattering tend to overestimate Γ and A_c due to the resolution limit. We believe that when the ranges of the parameters we found are used to fit the inelastic neutron scattering, highly accurate parameters can be found to comprehend the underlying magnetism and resolve the ongoing controversy on the existence and/or nature of the topological magnon gap. In addition, the two E_u phonon modes were measured at 1.5 K, which agreed with the DFT calculations. We verified the transformation of the phonon modes at the structural phase transition temperature in the presence of a magnetic field up to 7 T. The $R\bar{3}$-$C2/m$ boundary in bulk CrI_3 did not change with an external magnetic field. In conclusion, our THz-TDS spectra depending on temperature and external magnetic field effectively connect the optical properties of bulk CrI_3 with its magnetism. The magnetic Hamiltonian has been successfully analyzed in the combined Hamiltonian context, and the structure-field phase diagram of bulk CrI_3 established.

Methods

Sample preparation

Single crystals of CrI_3 were grown in situ via the chemical vapor transport method following the procedure described by McGuire et al.[8]. Chromium powder (99.99%, Alfa Aesar) and crystalline iodine (99.99%, Alfa Aesar) in a stoichiometric ratio with a slight amount of excess iodine (1% of total mass) were placed inside an evacuated quartz tubes and sealed. The typical dimensions of the quartz tubes were 100 mm in length, 10 mm in inner diameter, and 2 mm in thickness. The sealed quartz tube ampoules were heated to 650 °C/550 °C for one week in a two-zone furnace and cooled to room temperature. The sample stoichiometry of CrI_3 single crystal was verified by energy-dispersive X-ray (EDX) spectroscopy (Quantax 100, Bruker USA & EM-30, Coxem Korea).

Terahertz time-domain spectroscopy

A CrI_3 single crystal with a thickness of 217 μm was prepared via the mechanical exfoliation method and was fixed on an Au-coated Cu sample holder by using Kapton tape. The terahertz (THz) transmittance measurements were conducted by using a THz time-domain spectrometer (TERA K15, Menlo systems) over the frequency range of 1.5–120 cm^{-1}. The sample temperature varied from 4 to 290 K, and an external magnetic field aligned along the c and a axes up to 7 T was applied by using a He-free magneto-optic cryostat (Spectromag PT, Oxford Instruments). The temperature and external magnetic field dependence were measured while increasing the temperature and magnetic field after zero-field cooling.

Calculation

We performed linear spin-wave calculations to extract the expression for the energy gap observed in ferromagnetic resonance (FMR) of CrI_3. Initially, the classical magnetic ground state spin configuration was numerically determined by minimizing the total energy of the magnetic Hamiltonian. Then, we expressed the magnetic Hamiltonian in terms of the creation and annihilation operators of magnons up to the quadratic order with the spin configuration using the Holstein–Primakoff transformations. Finally, Fourier transformation allowed us to build the Hamiltonian in the momentum space and the equation of motion to calculate the FMR mode and absorbance[41]. The details are in the Supporting Information.

Data availability

The data that support the findings of this study are available from the corresponding author upon reasonable request.

Received: 23 January 2024; Accepted: 10 July 2024;
Published online: 20 July 2024

References

1. Lee, J.-U. et al. Ising-type magnetic ordering in atomically thin $FePS_3$. *Nano Lett* **16**, 7433–7438 (2016).
2. Huang, B. et al. Layer-dependent ferromagnetism in a van der Waals crystal down to the monolayer limit. *Nature* **546**, 270–273 (2017).
3. Gong, C. et al. Discovery of intrinsic ferromagnetism in two-dimensional van der Waals crystals. *Nature* **546**, 265–269 (2017).
4. Mermin, N. D. & Wagner, H. Absence of ferromagnetism or antiferromagnetism in one- or two-dimensional isotropic heisenberg models. *Phys Rev Lett* **17**, 1133 (1966).
5. Chen, L. et al. Topological Spin Excitations in Honeycomb Ferromagnet CrI_3. *Phys Rev X* **8**, 041028 (2018).
6. Chen, L. et al. Magnetic anisotropy in ferromagnetic CrI_3. *Phys Rev B* **101**, 134418 (2020).
7. Lee, I. et al. Fundamental spin interactions underlying the magnetic anisotropy in the kitaev ferromagnet CrI_3. *Phys Rev Lett* **124**, 017201 (2020).
8. McGuire, M. A., Dixit, H., Cooper, V. R. & Sales, B. C. Coupling of crystal structure and magnetism in the layered, ferromagnetic insulator CrI_3. *Chem Mater* **27**, 612–620 (2015).
9. McCreary, A. et al. Distinct magneto-Raman signatures of spin-flip phase transitions in CrI_3. *Nat Commun* **11**, 3879 (2020).
10. Huang, B. et al. Tuning inelastic light scattering via symmetry control in the two-dimensional magnet CrI_3. *Nat Nanotechnol* **15**, 212–216 (2020).
11. Guo, K. et al. Layer dependence of stacking order in nonencapsulated few-layer CrI_3. *Sci China Mater* **63**, 413–420 (2019).
12. Liu, Z. et al. Observation of nonreciprocal magnetophonon effect in nonencapsulated few-layered CrI_3. *Sci Adv* **6**, eabc7628 (2020).
13. Song, T. et al. Direct visualization of magnetic domains and moiré magnetism in twisted 2D magnets. *Science* **374**, 1140–1144 (2021).
14. Li, S. et al. Magnetic-field-induced quantum phase transitions in a van der waals magnet. *Phys Rev X* **10**, 011075 (2020).
15. Webster, L., Liang, L. & Yan, J. A. Distinct spin-lattice and spin-phonon interactions in monolayer magnetic CrI_3. *Phys Chem Chem Phys* **20**, 23546–23555 (2018).
16. Laulicht, I., Suss, J. T. & Barak, J. The temperature dependence of the ferromagnetic and paramagnetic resonance spectra in thin yttrium-iron-garnet films. *J Appl Phys* **70**, 2251–2258 (1991).
17. Fiebig, M. Revival of the magnetoelectric effect. *J Phys D: Appl Phys* **38**, R123 (2005).
18. Dillon, J. F. & Olsen, C. E. Ferromagnetic resonance of EuO. *Phys Rev* **135**, A434–A436 (1964).
19. Lee, S. et al. Ferromagnetic resonance of a YIG film in the low frequency regime. *J Appl Phys* **120**, 033905 (2016).
20. Farle, M. Ferromagnetic resonance of ultrathin metallic layers. *Rep. Prog Phys* **61**, 755 (1999).
21. Dillon, J. F. & Olson, C. E. Magnetization, resonance, and optical properties of the ferromagnet CrI_3. *J Appl Phys* **36**, 1259–1260 (1965).
22. Cenker, J. et al. Direct observation of two-dimensional magnons in atomically thin CrI_3. *Nat Phys* **17**, 20–25 (2021).
23. Do, S.-H. et al. Gaps in topological magnon spectra: Intrinsic versus extrinsic effects. *Phys Rev B* **106**, L060408 (2022).
24. Stavropoulos, P. P., Pereira, D. & Kee, H.-Y. Microscopic mechanism for a higher-spin kitaev model. *Phys Rev Lett* **123**, 037203 (2019).
25. Cen, J. & Kee, H.-Y. Strategy to extract Kitaev interaction using symmetry in honeycomb Mott insulators. *Commun Phys* **5**, 119 (2022).
26. Cen, J. & Kee, H.-Y. Determining Kitaev interaction in spin-S honeycomb Mott insulators. *Phys Rev B* **107**, 014411 (2023).
27. Chen, L. et al. Magnetic field effect on topological spin excitations in CrI_3. *Phys Rev X* **11**, 031047 (2021).
28. Stavropoulos, P. P., Liu, X. & Kee, H.-Y. Magnetic anisotropy in spin-3/2 with heavy ligand in honeycomb Mott insulators: Application to CrI_3. *Phys Rev Res.* **3**, 013216 (2021).
29. Belyaeva, A. I. & Eremenko, V. V. Temperature dependence of the optical absorption bandwidth of MnF_2 crystals. *Sov Phys JETP* **17**, 319–320 (1963).

30. Jennings, L. D. & Hansen, W. N. Heat Capacity of $CrBr_3$ from 14 to 360 °K. *Phys Rev* **139**, A1694–A1697 (1965).
31. Sivadas, N., Okamoto, S., Xu, X., Fennie, C. J. & Xiao, D. Stacking-dependent magnetism in bilayer CrI_3. *Nano Lett* **18**, 7658–7664 (2018).
32. Jiang, P. et al. Stacking tunable interlayer magnetism in bilayer CrI_3. *Phys Rev B* **99**, 144401 (2019).
33. Jang, S. W., Jeong, M. Y., Yoon, H., Ryee, S. & Han, M. J. Microscopic understanding of magnetic interactions in bilayer CrI_3. *Phys Rev Mater* **3**, 031001 (2019).
34. Tomarchio, L. et al. Low energy electrodynamics of CrI_3 layered ferromagnet. *Sci Rep.* **11**, 23405 (2021).
35. Larson, D. T. & Kaxiras, E. Raman spectrum of CrI_3: An ab initio study. *Phys Rev B* **98**, 085406–1 (2018).
36. Jin, W. et al. Observation of the polaronic character of excitons in a two-dimensional semiconducting magnet CrI_3. *Nat Commun* **11**, 4780 (2020).
37. Delugas, P., Baseggio, O., Timrov, I., Baroni, S. & Gorni, T. Magnon-phonon interactions enhance the gap at the Dirac point in the spin-wave spectra of CrI_3 2D magnets. *Phys Rev B* **107**, 214452 (2023).
38. Guiton, T. A. & Pantano, C. G. Infrared reflectance spectroscopy of porous silicas. *Colloids Surf A: Phpicochem Eng Asp* **74**, 33–46 (1993).
39. Kamitsos, E. I., Patsis, A. P. & Kordas, G. Infrared-reflectance spectra of heat-treated sol-gel-derived silica. *Phys Rev B* **48**, 12499–12505 (1993).
40. Niu, B. et al. Coexistence of magnetic orders in two-dimensional magnet CrI_3. *Nano Lett* **20**, 553–558 (2019).
41. Fishman, R. S., Fernandez-Baca, J. A. & Rõõm, T. Spin-Wave Theory and its Applications to Neutron Scattering and THz Spectroscopy. *IOP Concise Physics* (2018).

Acknowledgements

Research at Yonsei University was supported by National Research Foundation (NRF) grants funded by the Korean government (MSIT; Grants 2021R1A2C3004989 and 2020R1A6A3A01100029), the Nano & Material Technology Development Program (Ministry of Science and ICT; Grant number RS-2023–00281839). S. B. gratefully acknowledges the support received from the US DOE NNSA under Contract No.89233218CNA000001 through the LDRD Program. A portion of this work was performed at the National High Magnetic Field Laboratory, which is supported by the National Science Foundation Cooperative Agreement No. DMR-1644779 and the State of Florida and the U.S. Department of Energy. The calculation performed by M. L. is supported by the U.S. Department of Energy, Office of Science, National Quantum Information Science Research Centers. M. L. thanks Randy Fishman, Seung-Hwan Do and Shizeng Lin for helpful discussions. Work at Seoul National University was supported by the Leading Researcher Program of the National Research Foundation of Korea (Grant No. 2020R1A3B2079375). Kyung Ik Sim was supported by Institute for Basic Science (IBS-R011-D1).

Author contributions

Jonghyeon Kim, S.B., Junghyun Kim, and M.L. are the co-first authors. Jonghyeon Kim and Jae Hoon Kim conceived and designed the project. Jonghyeon Kim, S.B., Junghyun Kim, and M.L. performed most of the experiments, including the THz-TDS, linear spin-wave calculations, sample synthesis, and data analysis. S.S. performed the synthesis and magnetic susceptibility analysis. J.W., T.S.J., and K.I.S. performed THz-TDS analysis. Jonghyeon Kim, S.B., Junghyun Kim, M.L., J.G.P., and Jae Hoon Kim wrote the manuscript. J.G.P led the sample growth and characterization group; Jae Hoon Kim organized the measurement and analysis and led the experimental group. All the authors have discussed the results and commented on the manuscript.

Competing interests

The authors declare no competing interests.

Additional information

Supplementary information The online version contains supplementary material available at https://doi.org/10.1038/s41535-024-00666-y.

Correspondence and requests for materials should be addressed to Je-Geun Park or Jae Hoon Kim.